BLANKET ENGINEERING

KEYWORDS: *neutronics integral experiments, annular blanket, pseudoline source*

NEUTRONICS INTEGRAL EXPERIMENTS OF ANNULAR BLANKET SYSTEM SIMULATING TOKAMAK REACTOR CONFIGURATION

CHIKARA KONNO, YUKIO OYAMA, FUJIO MAEKAWA, YUJIRO IKEDA, KAZUAKI KOSAKO, and HIROSHI MAEKAWA
Japan Atomic Energy Research Institute, Department of Reactor Engineering
Tokai Research Establishment, Tokai-mura, Naka-gun, Ibaraki-ken, 319-11 Japan

MOHAMED A. ABDOU *University of California, Los Angeles*
School of Engineering and Applied Science
Mechanical, Aerospace, and Nuclear Engineering Department
Los Angeles, California 90095

EDGAR F. BENNETT *Argonne National Laboratory, Fusion Power Program*
Building 205, 9700 South Cass Avenue, Argonne, Illinois 60439

ANIL KUMAR and MAHMOUD Z. YOUSSEF
University of California, Los Angeles, School of Engineering and Applied Science
Mechanical, Aerospace, and Nuclear Engineering Department
Los Angeles, California 90095

Received September 29, 1994
Accepted for Publication March 29, 1995

Neutronics experiments on annular blanket systems that use a pseudoline source are performed. The shape of the annular blanket system is a rectangular parallelepiped (1300 × 1300 mm² and 2040 mm long) with an inner cavity of 425.5 × 425.5 mm² and 2040 mm long. The annular blanket consists of a 15-mm-thick first wall (Type 304 stainless steel) and 406-mm-thick breeder zone (inner lithium oxide and outer lithium carbonate). Deuterium-tritium neutron sources are set at the center of the inner cavity of the annular blanket system, and the pseudoline source is obtained by oscillating the annular blanket system back and forth in a 2-m span. Three annular blanket configurations are examined: the reference blanket, a blanket covered with 25-mm-thick graphite armor, and an armor blanket with a large opening (376 × 425.5 mm). The neutronics parameters of tritium production rate, neutron spectrum, and activation reaction rate are measured with specially developed techniques, including a multidetector data acquisition system, a spectrum weighting function method, and a ramp-controlled high-voltage system. Measured parameters are compared among three different configurations of the experimental system and also with the results of a closed geometry with a point source. A calculation with the GMVP Monte Carlo code that uses the JENDL-3 nuclear data library is performed and shows agreement within 10%. The current experiment provides unique data for a higher step of benchmark to test the ability of neutronics design calculations for a realistic tokamak reactor.

I. INTRODUCTION

A clean geometry for benchmarking or a composite prototypical setup for design verification of a fusion device are the two primary options of choice for an experimental blanket system. So far, many simple and small-scale integral neutronics experiments[1-3] have been conducted to validate nuclear data and calculation methods. Because a real fusion blanket design has a very complicated structure, a design calculation must be approximated more or less in a practical application. As long as the design reliability of a fusion reactor is

of interest, an integrated test that demonstrates the validity of the design parameters is important. An experimental configuration that resembles a real reactor as closely as possible is required. From this point of view, neutronics experiments on a variety of blanket configurations were performed in the Japan Atomic Energy Research Institute (JAERI)/U.S. Department of Energy (U.S. DOE) collaborative program on fusion blanket neutronics.[4-14] So far, those experiments have been performed in a geometry with a point neutron source.

A magnetic confinement machine such as a tokamak reactor, however, has a torus plasma and a toroidal blanket in which there is a source blanket geometry different from that in the case of a point source. All components relevant to the plasma core region, i.e., the structures of plasma elongation, divertor, limiter, inboard/outboard blankets, etc., impose an asymmetrical and three-dimensional geometry. This leads us to construct an annular test blanket with a line source for a prototypical mock-up of the tokamak reactor configuration. This geometry has an impact on neutronic features for the components near the plasma cavity because of multiangle neutrons incident to the blanket and multiple scattering of neutrons in the annular cavity. The pseudoline source was newly developed for the annular experiment.[15]

The experiments that used the line source and annular blanket system (Phase-III) were performed in the successive series of the JAERI/U.S. DOE collaborative program[16,17] to provide experimental data for validation of calculation capability in the three-dimensional geometry and configuration. Phase-III included measurement technique development suitable for the pseudoline source system and examination of the three-dimensional effects. The test assemblies were selected in three annular blanket configurations: (a) first wall/lithium oxide (Li_2O), (b) armor-first wall/Li_2O, and (c) armor-first wall/Li_2O with a large opening. The first blanket configuration functioned as the reference case with poloidal symmetry and axial (toroidal) uniformity. The second and third configurations simulated a graphite armor plate for protection of the first wall from energetic ions and an opening hole for a neutral beam injector, respectively. This paper summarizes all the experimental procedures and examines the effects of various configurations on neutronics parameters such as the tritium production rate (TPR). Typical calculations that used the recent GMVP Monte Carlo code[18] were also tested by comparison with the measured values.

II. EXPERIMENTAL ARRANGEMENT

II.A. Line Neutron Source and Setup

A line neutron source was adopted by the superposition technique in which a moving point source inside the annular blanket forms a pseudoline source by time averaging. This superposition was also obtained from a number of the distributed point sources. This system was realized by the annular test blanket moving relative to the fixed deuterium-tritium (D-T) point source over a 2-m span.[15] The experimental system was installed in the large irradiation room of the Fusion Neutronics Source (FNS) facility[19] at JAERI. The room is 15 m square and 9 m high, and the floor is made of steel grating at a height of 3 m from the base floor.

Two operational modes of the carriage deck were adopted in the experiment: the stepwise and the continuous modes. In the stepwise mode, the carriage deck was stopped every 50 or 100 mm over a 2-m length, and the detector signals were collected during the pause as the source positionwise data. This mode was applied to on-line measuring techniques such as NE-213 and Li-glass scintillators and the proton-recoil gas proportional counter (PRC). In the continuous mode, the test blanket continuously moved forth and back with a constant speed of 6.1 mm/s. The position of the carriage deck and the neutron yield were recorded every 10 s. This mode was applied to a passive technique that requires high neutron fluence such as activation foil measurements.

A cup-shaped tritium-titanium metal target with a long drift tube 2.3 m in length was specially made to insert into the annular test blanket. The target of 370 GBq tritium cooled by water was bombarded by a deuteron beam of 0.1 to 2 mA with 350 keV. The D-T neutron generation rate was monitored by a surface-barrier silicon detector that counted alpha particles produced from a $^3T(d,n)^4He$ reaction.[20] The detector was installed inside the beam drift tube 2.98 m from the target. The measured data were normalized by the neutron yield of the source at each stationary position for the stepwise mode and by the total number of neutrons emitted during the continuous irradiation with a decay correction for the continuous mode.

II.B. Annular Test Blankets

The test blanket was placed on a large 3.4- × 8-m carriage deck that was moved on four rails by a computer-controlled servomotor drive system. The test assembly was constructed from rectangular blocks of materials to maintain flexibility for making various configurations. The blocks piled up for the annular test blanket were secured by aluminum frames.

II.B.1. Reference Test Blanket (Phase-IIIA)

Figure 1 shows the cross section of the reference test blanket, named the Phase-IIIA assembly, which was made with a simple configuration that simulated only the first wall and the breeder zone. The assembly was constructed of blocks with unit sizes: Li_2O blocks covered with 0.3-mm-thick stainless steel with a 50.6-mm unit or its multiples and lithium carbonate (Li_2CO_3)

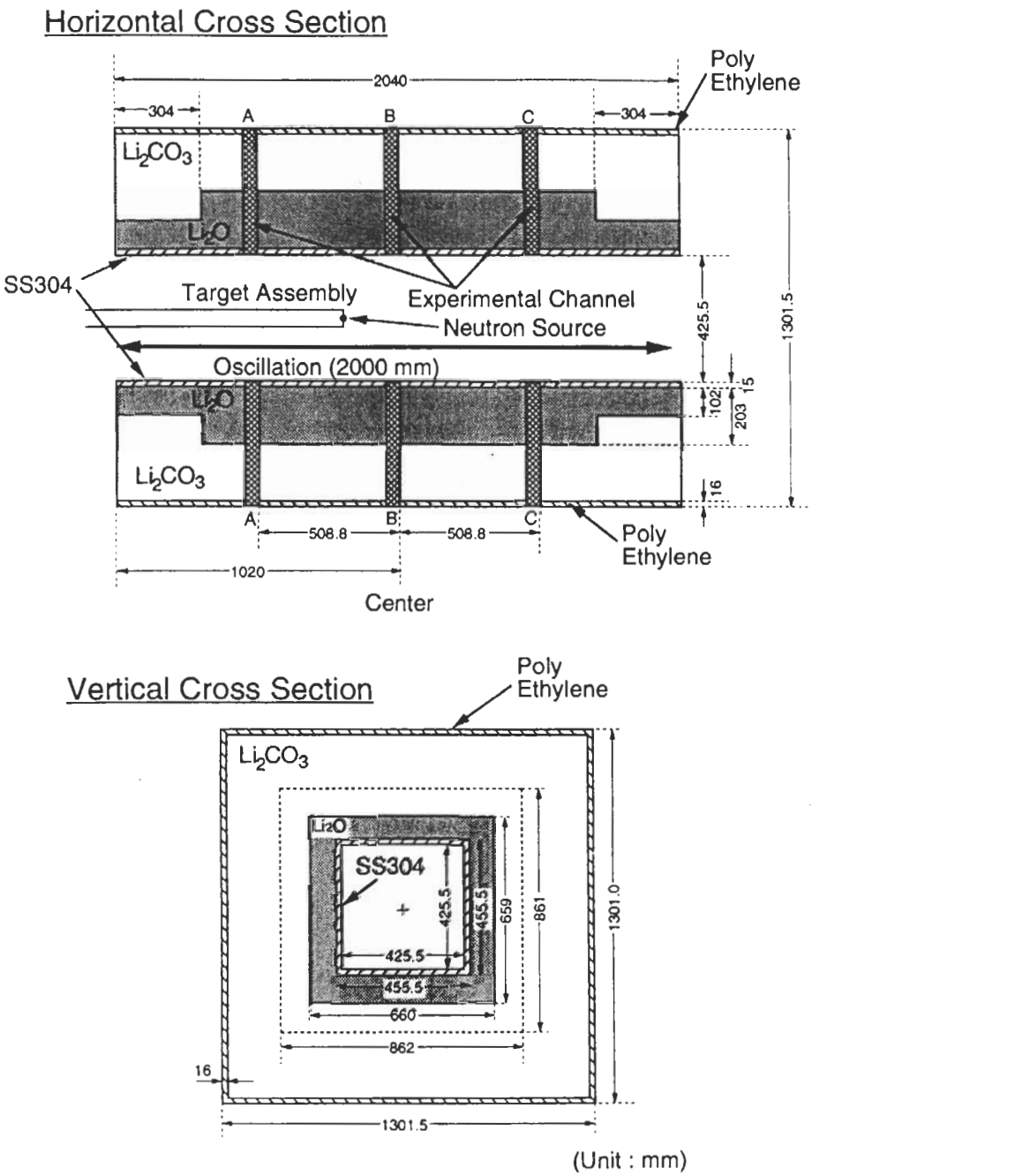

Fig. 1. Cross section of the reference configuration of annular test blanket assembly (Phase-IIIA).

blocks painted with epoxy paint with a 101.2-mm unit. The 0.3-mm-thick stainless steel and the epoxy paint were adopted to protect the Li_2O and the Li_2CO_3 bricks, respectively, from humidity in the atmosphere. Lithium oxide is a promising candidate for breeding material, and the front part of the breeding zone was rather important in this experiment. However, because Li_2O is a very expensive material, the Li_2O was placed inside the blocks and surrounded by Li_2CO_3 at the outer 203-mm-thick region. The Li_2CO_3 blocks also worked as a buffer zone in the outer blanket region to adjust the boundary conditions because of similar nuclear performance. The outer surface of the Li_2CO_3 region was covered with 16-mm-thick polyethylene plates to reduce the room-return neutrons. Type 304 stainless steel plates that were 15-mm-thick were placed inside the Li_2O region to simulate the first wall. The plates also supported the upper part of the assembly. The distance between the first-wall surface and the line source was 213 mm. The size of the internal cavity was

425.5 × 425.5 mm^2 and 2040 mm long. The D-T point source traversed the central axis of this cavity.

Three experimental channels for in situ measurements were installed horizontally in each side of the assembly and were separated from each other by a 509-mm axial distance. The channels were made of a 0.3-mm-thick sheath of Type 304 stainless steel for insertion of the special blocks (named drawers A, B, and C from the target side). These blocks were a little smaller than the normal blocks used in the assembly construction and had a 20-mm^2 hole for insertion of a detector for measurement. Table I summarizes the homogenized atomic densities of the materials used in the test blanket.

II.B.2. Armor Test Blanket (Phase-IIIB)

In a basic design of the the International Thermonuclear Experimental Reactor (ITER) Conceptual Design Activity phase, carbon fiber composite tiles that are 20 mm thick are attached to a few millimetres thick stainless steel plate in front of the first wall.[21] To simulate this kind of graphite armor as a typical plasma-facing component, a 25-mm-thick graphite layer was placed on the cavity surface in addition to the first wall of the reference test blanket. The graphite armor would play the roles of moderator and reflector to increase lower energy neutrons inside of the cavity. The 25-mm-thick and 50.8- × 203.2-mm^2 graphite blocks were piled up inside the cavity with aluminum spacers. The ceiling part of the graphite blocks was supported by 1-mm-thick aluminum plates. The atomic density of the graphite used was 1.652 g/cm^3. The other parts were completely the same as the reference test blanket including the experimental channel structure. The dimensions and cross sections of this test assembly are shown in Fig. 2.

TABLE I

Atomic Densities of Materials Used in Phase-III Series

Material	Element	Atomic Density (atom/cm^3)
Type 304 stainless steel	Iron	6.0210×10^{22}
	Chromium	1.5302×10^{22}
	Nickel	8.2258×10^{21}
	^{55}Mn	1.2607×10^{21}
Li_2O block[a]	^{6}Li	4.1921×10^{21}
	^{7}Li	5.2411×10^{22}
	^{16}O	2.8302×10^{22}
	Chromium	3.0188×10^{20}
	^{55}Mn	1.5440×10^{19}
	Iron	1.0976×10^{21}
	Nickel	1.3358×10^{20}
Li_2CO_3 block	^{6}Li	2.2798×10^{21}
	^{7}Li	2.8030×10^{22}
	^{12}C	1.5155×10^{22}
	^{16}O	4.5464×10^{22}
Polyethylene	Hydrogen	8.2560×10^{22}
	^{12}C	4.1280×10^{22}
Graphite	^{12}C	8.2894×10^{22}

[a]This includes the stainless steel can.

II.B.3. Large Opening Test Blanket (Phase-IIIC)

In a realistic reactor, there are many ports and ducts for plasma diagnostics, neutral beam injection (NBI), vacuum pumping, etc. These openings and holes, especially large openings for NBI, will influence the nuclear parameters around the ports because of leakage of neutrons and reduction of reflected neutrons. For example, a coverage factor for estimating the tritium breeding ratio should take into account the opening effect. A simple area fraction has been used so far for a factor to obtain the tritium breeding ratio in a whole reactor from the local breeding ratio calculated by a one-dimensional code. Because the opening structure cannot be treated by such a simple calculation, the current experiment provides a good three-dimensional benchmark for precise calculations by sophisticated transport codes.

A 376- × 425.5-mm^2 opening was made in the middle of the armor test blanket (Phase-IIIB) and was lined in the same way as the cavity with 15-mm-thick Type 304 stainless steel, as shown in Fig. 3. The inner surface of the opening was not covered with the graphite. The experimental channels were changed for the opening side; one channel was placed beside the opening and named drawer D. Figure 4 shows a photograph of the opening at the side of the assembly.

III. MEASUREMENTS

The quantities measured in the experiments were TPR, the neutron spectrum, and reaction rate. The experimental channels previously described, were used to perform the measurements. Reaction rate distributions in the inner cavity surface were also measured to examine the neutron flux distribution in the cavity. For the TPR measurement, a pair of ^{7}Li-enriched and ^{6}Li-enriched glass scintillators[22] and an indirect NE-213 scintillation detector method[23] [that used an evaluated value of the $^{7}Li(n,n'\alpha)^{3}T$ cross section] were applied for the on-line measurements. The stepwise operation mode of the line source was used for these detectors. The neutron spectrum was measured by the NE-213 scintillator[23] and a PRC (Ref. 24) with the stepwise operation mode. Two kinds of PRCs filled with gases of hydrogen and hydrogen/argon were applied as in the previous experiments[8,13] to cover the range from a few kilo-electron-volts to 1 MeV. In the latter case, the argon gas was used to increase the stopping power of the

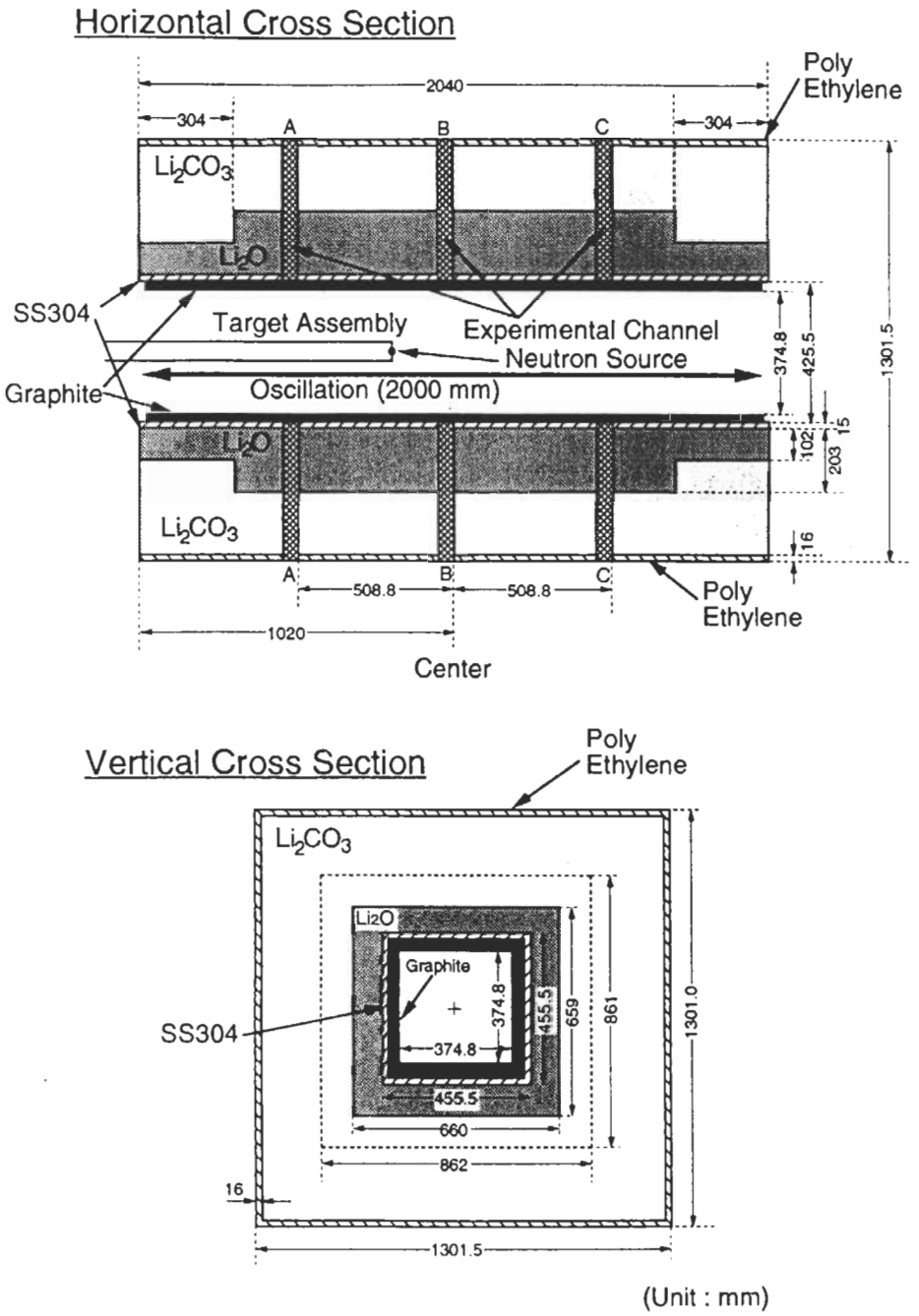

Fig. 2. Cross section of the armor test blanket assembly (Phase-IIIB).

recoil protons. The reaction rates were obtained by the activation foil method with the continuous operation mode of the line source.

These are almost the same techniques as used in the previous experiments[7,8,13] in the JAERI/U.S. DOE collaboration program that used a point neutron source, i.e., Phases-I and -II. However, to apply them to the current line source experiment, we introduced the following modifications or new techniques to improve the measurements:

1. ramp high-voltage application and data acquisition system for PRC
2. multidetector data acquisition system for the Li-glass
3. spectrum weighting function method for the NE-213 detector
4. flux variation and gamma-ray decay correction for activation foil technique.

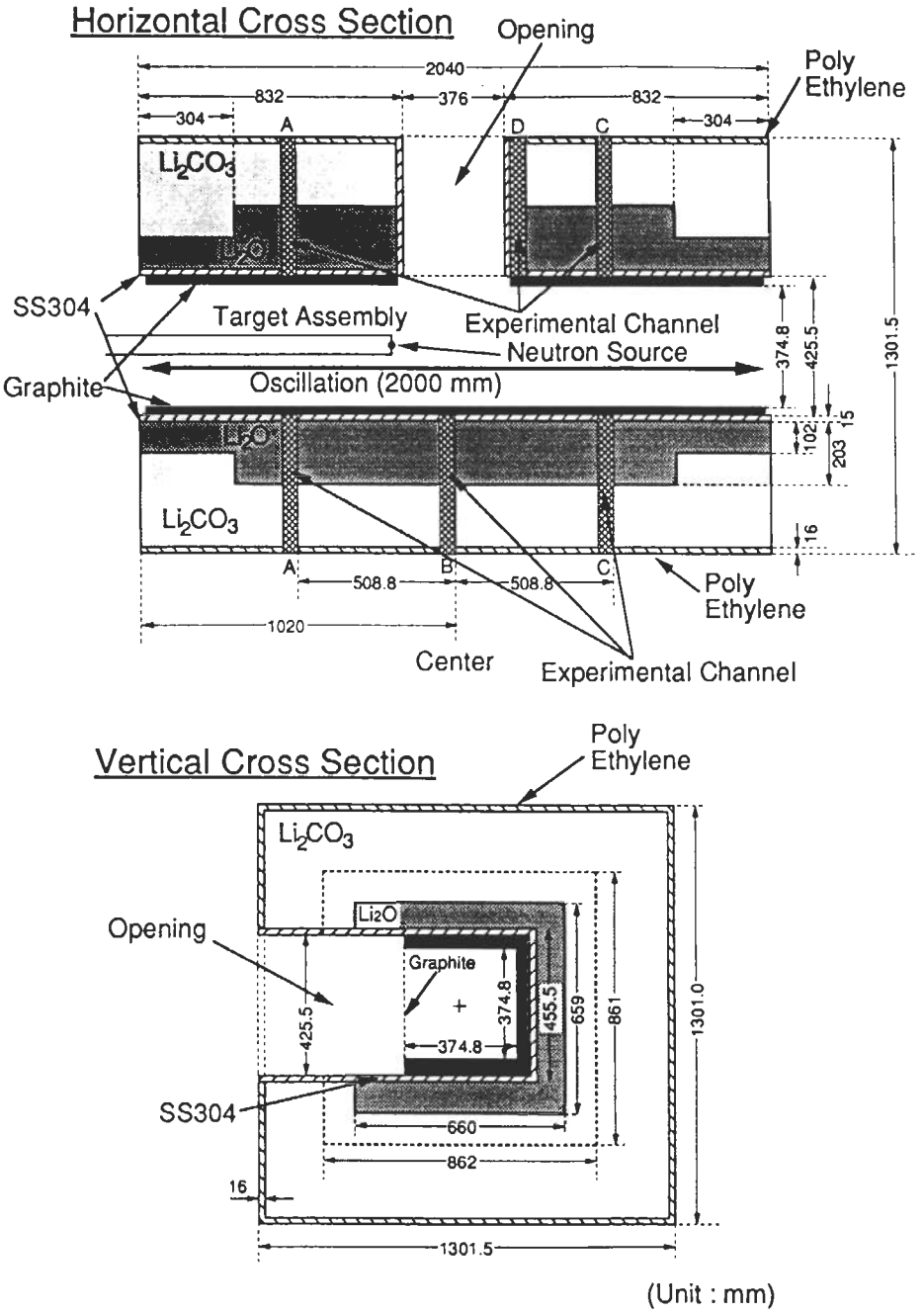

Fig. 3. Cross section of large opening test blanket assembly (Phase-IIIC).

The last technique is explained in Ref. 15 with the source characteristics experiment. The other techniques are described in the following sections.

III.A. PRC with Ramp High-Voltage Operation

A new technique[25] for PRC was developed to reduce the time of measurement and data processing. In the conventional technique, several high-voltage runs are separately performed for one measurement, but the new technique could take data in a single measurement run by using a high-voltage sweep with a ramp shape. This significantly reduced the measurement time and allowed us to apply the PRC technique to the experiment in the stepwise mode of the line source. In that mode, a large number of measurements were needed corresponding to the number of sources.

The voltage was scanned from 3000 to 4200 V for the hydrogen counter and from 2400 to 3000 V for the hydrogen/argon counter in 165 s for one cycle, and

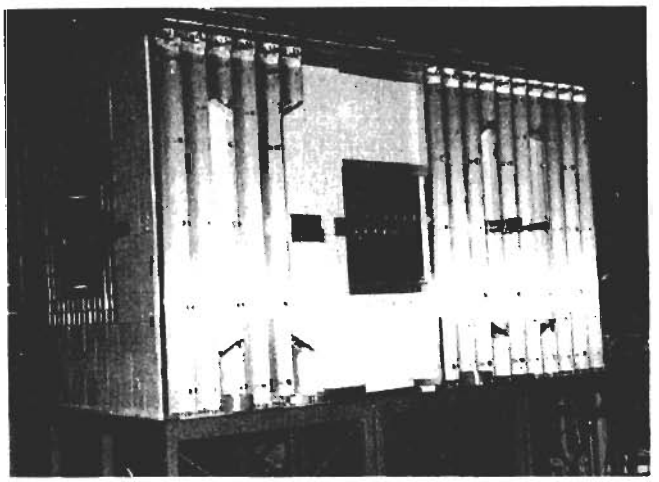

Fig. 4. Photograph of large opening test blanket assembly (Phase-IIIC).

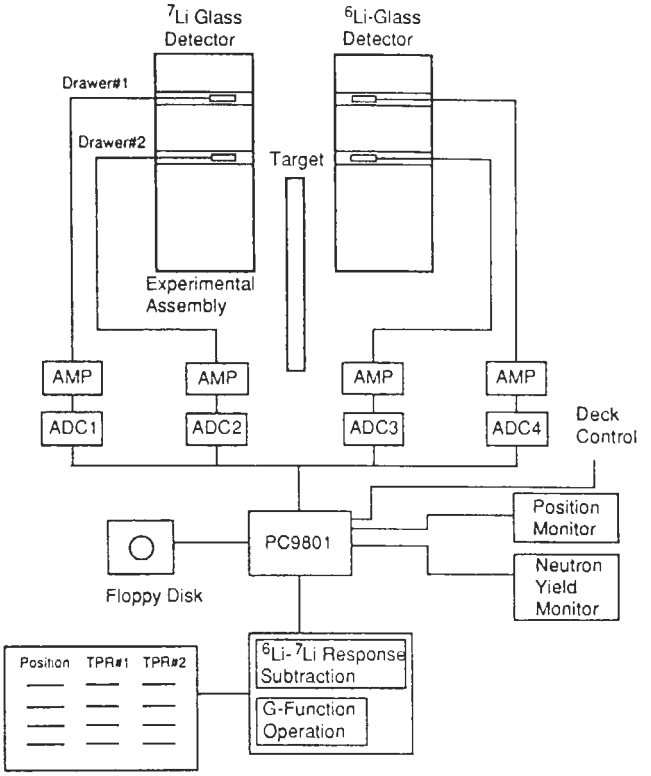

Fig. 5. Multidetector data acquisition system for simultaneous measurement of ^{7}Li- and ^{6}Li-glass detectors.

six cycles were performed for the measurement at 20 source positions with 100-mm interval. The detector signals were collected in three-dimensional data with coincidence of applied voltage, rise time, and pulse height. The pulse-height signals from the neutrons were separated from the gamma-ray signals by using the difference of rise time for each signal (pulse-shape discrimination). The pulse-height signals from the neutrons were converted to the recoil proton energy by using a gas multiplication factor corresponding to the supplied voltage recorded at the same time. The neutron spectrum was finally obtained by differentiation of the recoil proton spectrum. With this innovative technique, the recoil proton spectrum in the whole energy range could be taken without any connection of several measurement runs that used different supplied voltages.

III.B. Li-Glass with Multidetector Data Acquisition

For a Li-glass detector, a background subtraction measured with the ^{7}Li-glass scintillator was necessary to obtain the TPR from ^{6}Li. Utilizing the symmetric geometry of the annular blanket, we placed a pair of detectors of ^{7}Li- and ^{6}Li-glass scintillators, each which had a 10-mm diameter and a 0.3-mm thickness, in a symmetrical position in experimental drawers on both sides. As illustrated in Fig. 5, two pairs of Li-glass detectors were set to obtain the data at two positions at the same time. The measurement time was 1000 s for one source position. When the source was moved from one end of the assembly to the other, the background fraction due to the gamma rays from the materials around the detector became higher after the source passed the detector position because the gamma-ray flux increased as a result of production of short-lived activities and the neutron flux decreased with increasing distance from the source. Hence, the beam current was kept lower even in the source position far from the detector. Four pulse-height spectra were taken for one source position to obtain the TPR at two detector positions, and those were repeated for 21 source positions with 100-mm intervals.

III.C. NE-213 Detector with Spectrum Weighting Function Method

The spectrum weighting function method[26] was used to obtain TPR of ^{7}Li and the integrated neutron flux above 10 MeV from the pulse-height spectrum measured by a small sphere NE-213 liquid scintillation detector.[23] This method can deduce the nuclear parameter in a simpler way than a spectrum unfolding technique. When one must process a large number of data at the same time, this method reduces the measurement and data processing time. Because the spectrum weighting method works well even in low counting statistics, the positionwise data processing became practical in spite of the short acquisition time at each source position.

By using the spectrum weighting function method, nuclear parameter R is given by

$$R = \int C(H_p) \cdot W(H_p)\, dH_p \ ,$$

where $C(H_p)$ is a recoil proton energy spectrum measured by the NE-213 spectrometer and $W(H_p)$ is a

spectrum weighting function that is calculated by the neutron response matrix of the detector and the energy response to be measured. The weighting function can be calculated for many kinds of nuclear responses $F(E_n)$ that are sensitive to high-energy neutrons such as the tritium production cross section, the displacements-per-atom cross section, gamma heating, etc. In addition, by utilizing the foregoing multidetector data acquisition system, three NE-213 scintillation detectors were applied at the same time for three experimental channels.

The result could be obtained simply by multiplying the measured pulse-height spectrum by the weighting function. The statistical error of the results by the spectrum weighting function method almost followed the total counts for the detector. However, the accuracy of the results depends on the energy response data, i.e., the cross section, the neutron and gamma-ray kerma, etc. In the current experiments, the TPRs from ^{7}Li and the integrated flux above 10 MeV were deduced by this method. On the other hand, to obtain the energy spectrum, a conventional unfolding technique was applied with the FORIST code[27] by summing up the pulse-height spectra normalized by each neutron yield for all source positions.

III.D. Activation Foil Detector

In the continuous operation mode of the line source, the neutron flux at the foil position varies with the source position, i.e., the distance between the source and the detector. This causes time variation of the neutron flux during irradiation. For the activation reactions with shorter decay times, a correction is necessary to deduce the reaction rate for the line source from the observed response because the assumption of the superposition by time averaging is not valid exactly. This correction was performed in the same way as the source characteristics experiment,[15] although the neutron attenuation in the test blanket had to be neglected. Because if the correction is small, the error due to neglecting is also small, this approximation is reasonable for most reactions. The activation reactions used are summarized in Table II. The sizes of the foils were 10 to 20 mm in diameter and 1 mm in thickness, and for gold, a thin foil of 1-μm thickness was used to avoid a self-shielding effect.

IV. EXPERIMENTAL RESULTS AND DISCUSSION

IV.A. Experimental Results and Comparison Among Experimental Results

IV.A.1. TPR

The TPRs from ^{7}Li and ^{6}Li (T_7 and T_6) were measured separately by the NE-213 and Li-glass scintillators, respectively. Because both the on-line methods utilized the stepwise mode line source operation, the source positionwise TPRs (named as the source profile) were obtained at the same time. Figure 6 shows the source profiles of T_7 by the NE-213 in drawer B (mid position) 227 and 393 mm from the source traveling line. Though the source profiles inside the blanket were similar to each other, there were some differences between the blankets with and without graphite armor, corresponding to Phases-IIIB and -IIIA, respectively. By the graphite layer, T_7 decreased at both ends because

TABLE II

Dosimetry Reactions Used in the Experiments

Reactions	Half-Life	Abundance (%)	Gamma-Ray Energy (keV)	Gamma-Ray Branching (%)	Threshold Energy (MeV)	Typical Foil Size (mm)
^{27}Al$(n,\alpha)^{24}$Na	15.02 h	100.0	1368.6	100.0	5	15 diam × 1
^{nat}Ti$(n,x)^{46}$Sc	83.83 days	100.0	889.3	99.98	4	20 diam × 1
^{nat}Ti$(n,x)^{47}$Sc	3.341 days	100.0	159.4	68.0	1.5	20 diam × 1
^{nat}Ti$(n,x)^{48}$Sc	1.821 days	100.0	983.5	100.0	5	20 diam × 1
^{55}Mn$(n,\gamma)^{56}$Mn	2.579 h	100.0	846.8	98.9	---	12.7 diam × 0.05
^{54}Fe$(n,p)^{54}$Mn	312.2 days	5.8	834.8	99.98	2	10 diam × 1
^{58}Ni$(n,p)^{58}$Co	70.92 days	68.3	810.8	99.5	2	15 diam × 1
^{58}Ni$(n,2n)^{57}$Ni	1.503 days	68.3	1377.6	77.9	12.5	15 diam × 1
^{59}Co$(n,\alpha)^{56}$Mn	2.579 h	100.0	846.8	98.9	6	10 diam × 1
^{64}Zn$(n,p)^{64}$Cu	12.70 h	48.6	511.0	74.2	1.5	20 diam × 1
^{90}Zr$(n,2n)^{89}$Zr	3.268 days	51.45	909.2	99.01	12	20 diam × 1
^{93}Nb$(n,2n)^{92m}$Nb	10.15 days	100.0	934.5	99.0	9	20 diam × 1
^{115}In$(n,n')^{115m}$In	4.486 h	95.7	336.3	45.8	0.34	10 × 10 × 1
^{197}Au$(n,\gamma)^{198}$Au	2.694 days	100.0	411.8	95.5	---	10 × 10 × 0.001

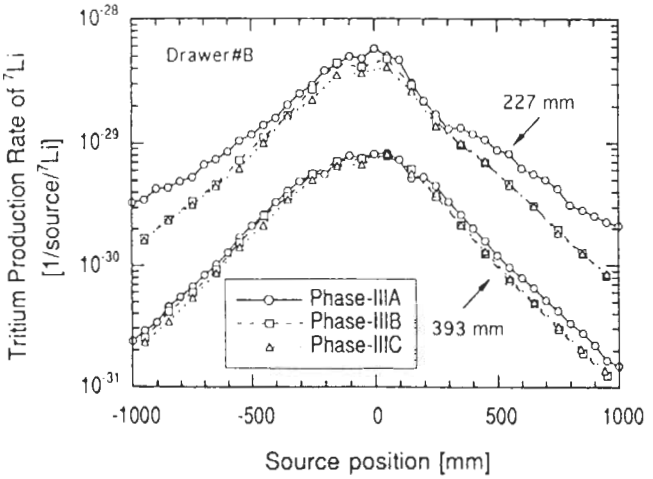

Fig. 6. Source positionwise TPR profile of ^{7}Li measured by the NE-213 detector at positions 227 and 393 mm from the line source of central drawer B for three blankets.

the effective thickness of the graphite increased because of the oblique incident. In a comparison of the opening blanket (Phase-IIIC) with the nonopening blanket (Phase-IIIB), T_7 decreased at the mid region because of a decrease of reflected neutrons. At the forward region, there was a structure in the profile for the reference blanket (Phase-IIIA). This structure was seen only for the reference (Phase-IIIA). Thus, this could be explained as follows: Parasitic neutrons by a $D(d,n)^3He$ reaction with a beam flare on the step of the drift tube created the second neutron source ~200 mm from the target. The contribution was not so large that the effect on the superposed TPR could be neglected. There was no flare in the other experiments (Phases-IIIB and -IIIC) because beam tuning might be fine.

Figure 7 shows the source profiles of T_6 measured by the Li-glass detector in drawer B 279 and 380 mm from the source traveling line. The T_6 profiles were broader than the T_7 profiles because the T_6 profile was not dominated by an inverse square law of the distance from the target. The width of the T_6 profile was two times larger than that of the T_7 profile. The effect of the armor layer, a 10% increase of TPR, spread to the whole blanket region, especially at the front region and at the center. However, the effect of the opening was only in the region comparable with the opening size. This meant that the opening effect on T_6 was caused by a change in the number of reflected neutrons and was contrary to the $^{197}Au(n,\gamma)$ reaction on which the opening effect spread over the cavity along the whole line source, as discussed in Sec. IV.A.3.

The TPRs from ^{7}Li and ^{6}Li (T_7 and T_6) for the line source were reduced by superposing the source profile data in drawer B. The results are shown in Fig. 8 and summarized in Tables III and IV. The distributions along the radial axis were measured in each drawer. The T_7 distribution was steeper than that of the previous

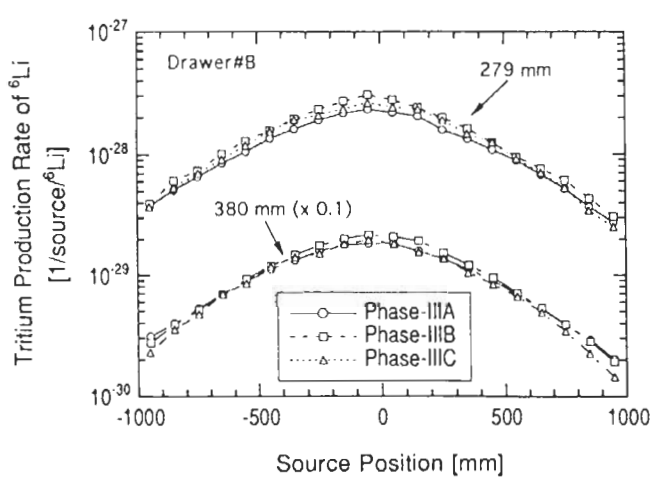

Fig. 7. Source positionwise TPR profile of ^{6}Li measured by the Li-glass detector at positions 279 and 380 mm from line source of central drawer B for three blankets.

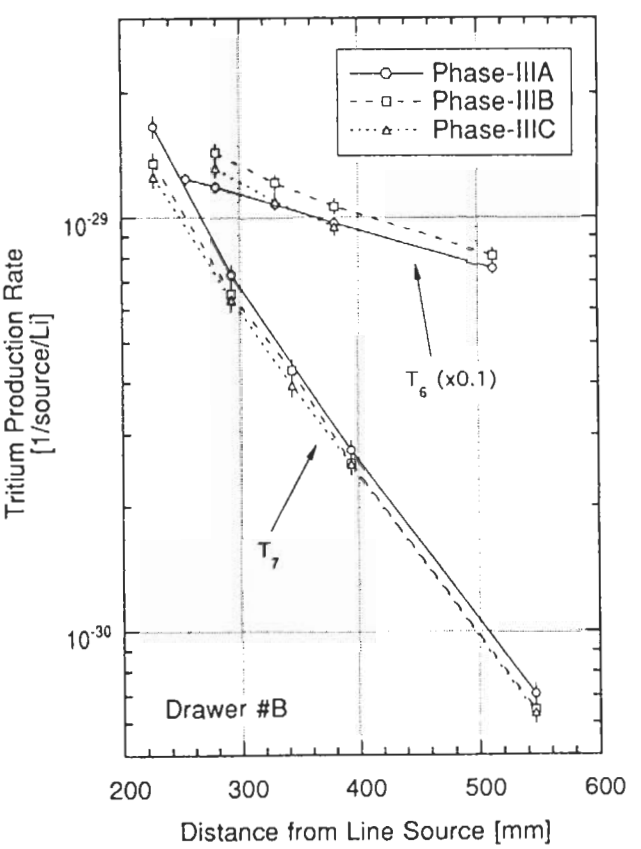

Fig. 8. Radial distribution of TPRs of ^{7}Li and ^{6}Li (T_7 and T_6) measured by the NE-213 and Li-glass detector in drawer B for three blankets.

TABLE III

TPR of ^{7}Li for the Line Source Measured by the NE-213 Detector

Position (mm)	Phase-IIIA TPR-^{7}Li	Error (%)	Phase-IIIB TPR-^{7}Li	Error (%)	Phase-IIIC TPR-^{7}Li	Error (%)
B Drawer						
216.80	1.659E−29[a]	6.1	---	---	---	---
226.70	---	---	1.355E−29	6.2	1.256E−29	5.9
292.40	7.257E−30	6.0	6.541E−30	6.2	6.334E−30	6.5
343.40	---	---	4.284E−30	6.2	3.945E−30	6.3
393.40	2.747E−30	6.0	2.550E−30	6.1	2.539E−30	6.1
545.80	7.063E−31	6.0	6.468E−31	6.0	6.334E−31	6.0

[a]Read as 1.6590×10^{-29} (reaction/total source neutron/lithium).

TABLE IV

TPR of ^{6}Li for the Line Source Measured by the Li-Glass Detector

Position (mm)	Phase-IIIA TPR-^{6}Li	Error (%)	Phase-IIIB TPR-^{6}Li	Error (%)	Phase-IIIC TPR-^{6}Li	Error (%)
B Drawer						
254.0	1.244E−28[a]	4.9	---	---	---	---
279.4	1.188E−28	4.5	1.436E−28	5.0	1.319E−28	4.9
329.8	1.074E−28	4.3	1.213E−28	4.7	1.094E−28	4.7
380.4	9.672E−29	4.3	1.063E−28	4.6	9.488E−29	4.8
512.2	7.494E−29	4.3	2.550E−30	4.5	---	---

[a]Read as 1.2435×10^{-28} (reaction/total source neutron/lithium).

experiments[8] with a point source (Phase-IIA) because this gradient was mainly dominated by the distance between the source and the test blanket. The T_7 distributions in the armor and the opening blankets (Phases-IIIB and -IIIC) were ~10% smaller than that of the reference (Phase-IIIA) because of scattering at the 25-mm-thick graphite layer, but there was no effect at the opening. On the other hand, the T_6 distributions were flatter than those of the Phase-IIA experiment. The distributed incident source neutrons compensated the low-energy neutrons leaking from the measured region. In comparison among the different configurations, T_6 increased much by the graphite layer but decreased almost by the same amount because of the opening. This was consistent with the result of the T_6 profile at the middle region.

IV.A.2. Neutron Spectrum

Neutron spectra above 2 MeV and from a few kiloelectron-volts to 1 MeV were measured by the NE-213 scintillator and PRC with the stepwise line source mode, respectively. The data were taken at every 100-mm step of the source position. The raw pulse height spectra of the recoil protons were summed up, and then they were unfolded to obtain the neutron spectra. This procedure was applied only to the selected positions, the surface of the test region and the position 79.4 mm from the surface of the first wall, where the measurements by both PRC and the NE-213 were performed.

The measured spectrum at the annular test blanket surface with a line source are compared in Fig. 9 with the experiment[8] of a closed geometry with a point source (Phase-IIA). Because the spectrum of the point source experiment was obtained at the forward direction, the mean energy of the peak above 10 MeV was almost 14.8 MeV because of D-T reaction kinematics. On the other hand, the dominant energy of the line source was 14.1 MeV because neutrons emitted to the direction of 90 deg, and the peak was broader because of the contribution of neutrons from various emission angles. These mean energy and broadness of the peak spectra are more similar to a neutron source that is produced in a fusion device.

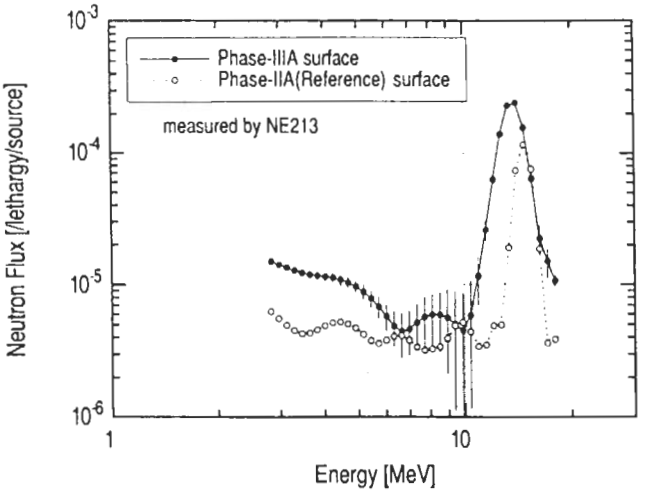

Fig. 9. Comparison of source neutron spectra measured at the surface of test blanket between the Phase-II point source experiment and the Phase-III line source experiment.

The spectra at the front surface and the inside (at a depth 79.4 mm from the first-wall surface) of the test blanket in the reference (Phase-IIIA) are compared in Fig. 10. The calculated neutron spectra described in Sec.IV.B are also shown in Fig. 10. The difference of the spectra at the two positions was seen in the range above 200 keV where the neutron flux at the inside decreased by less than one-half. Below 200 keV, the flux was almost the same, but the resonances for iron at the surface and for lithium at the inside are seen. The spectra between the reference (Phase-IIIA) and the armor (Phase-IIIB) experiments are compared at a depth 79.4 mm from the first-wall surface (292.4 mm from the line source) in Fig. 11. Both spectra are very similar, although a dip due to the resonance of the $^6Li(n,\alpha)^3T$ reaction at 250 keV was somewhat sharper for the armor blanket. Figure 12 shows the comparisons of the lower energy spectra measured by PRC at the surfaces of the opening and normal sides for the opening test blanket (Phase-IIIC). The higher energy part ($En \geq 2$ MeV) by the NE-213 was not measured because the same spectra as the armor blanket experiment (Phase-IIIB) were expected. Figure 12 indicates that the spectrum at the side with the opening hole was lower by

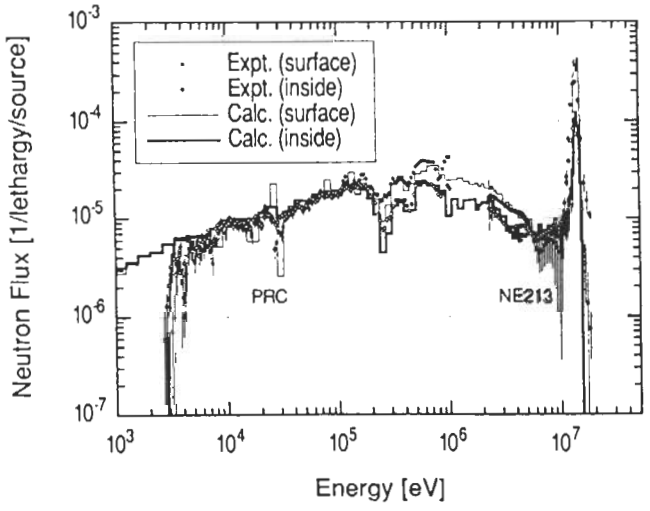

Fig. 10. Measured spectra at the surface and inside of the reference blanket by the NE-213 and the PRC spectrometers. Calculated spectra by GMVP are also plotted.

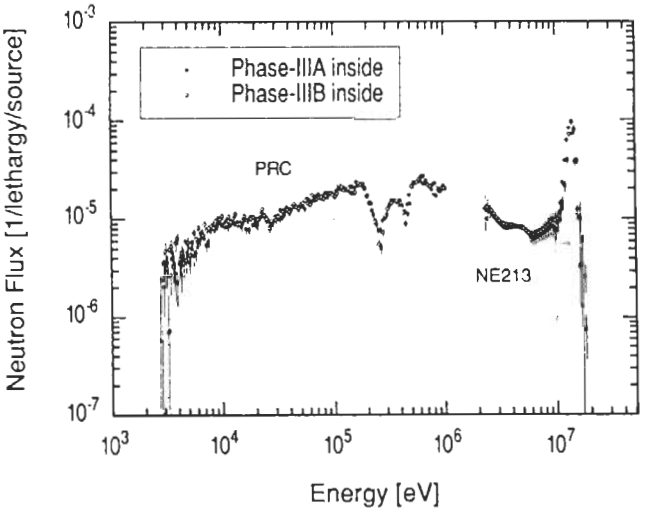

Fig. 11. Measured spectra inside the blanket for the reference (Phase-IIIA) and the armor (Phase-IIIB) test blankets.

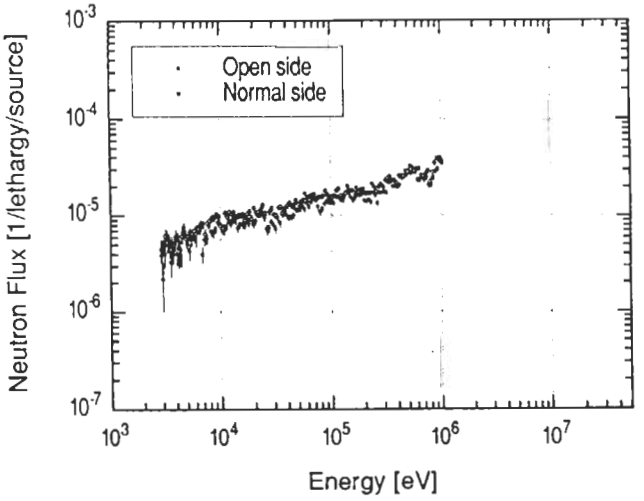

Fig. 12. Measured spectra at the surfaces of both the opening and the normal sides for ^6Li.

~10% than that at the other side. This was because there were no neutrons reflected from the graphite armor at the opening side.

IV.A.3. Activation Reaction Rate

We performed the measurements of the reaction rates with the activation foil method in two directions: along the line source axis on the cavity surface and along the radial axis using the experimental drawers. For the opening test blanket experiments, the measurement was performed on both surfaces at the normal and the opening sides.

The reaction rates of $^{93}Nb(n,2n)^{92m}Nb$, $^{115}In(n,n')^{115m}In$, and $^{197}Au(n,\gamma)^{198}Au$ were compared among the experimental assemblies as the typical reactions because the threshold energies of those reactions were 9 MeV, 335 keV, and thermal, respectively. Figures 13 and 14 show the measured reaction rate distributions along the line source at the surface of the test region. The distance from the source to the foils in the reference (Phase-IIIA) was adjusted to 219 mm by setting the foils 50 mm below the horizontal plane of the line source while the distance from the line source to the foils in the armor and the opening blanket (Phases-IIIB and -IIIC) was 187 mm because the graphite was added to the surface of the first wall. The reaction rates in the armor blanket (Phase-IIIB) were larger than those in the reference (Phase-IIIA) because of the shorter distance while the reaction rates of $^{197}Au(n,\gamma)^{198}Au$ increased more than those expected as a result of the shorter distance because the armor graphite increased low-energy neutrons inside the cavity eminently. The reaction rates of the $^{197}Au(n,\gamma)^{198}Au$ reaction decreased because of the opening hole effect in the opening blanket (Phase-IIIC). Note that the opening effect spread over the cavity, in contrast to TPR from ^{6}Li. Figure 15 shows the measured reaction rate distributions along the line source on both sides of the opening blanket (Phase-IIIC) surfaces: the hole side and the no-hole side. For $^{93}Nb(n,2n)^{92m}Nb$ (high-threshold reaction), there is not a significant difference between the two sides while for $^{115}In(n,n')^{115m}In$ and $^{197}Au(n,\gamma)^{198}Au$, a decrease of the reaction rate is clearly observed in the region corresponding to the width of the opening hole.

Tables V, VI, and VII show the measured reaction rate radial distributions in experimental drawer B. The reaction rates of $^{93}Nb(n,2n)^{92m}Nb$, $^{115}In(n,n')^{115m}In$,

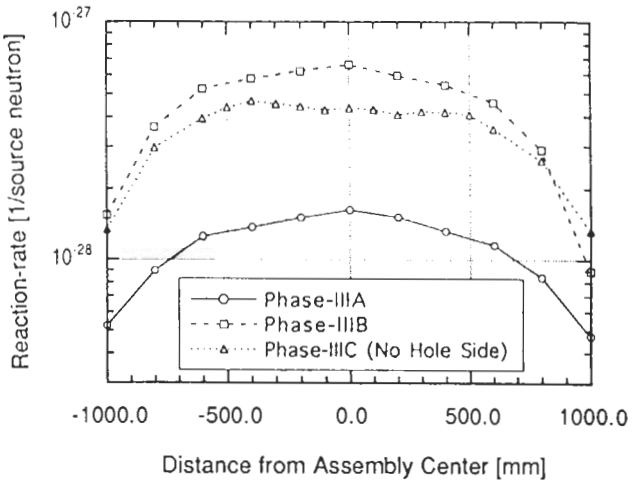

Fig. 14. Activation reaction rate distribution of $^{197}Au(n,\gamma)^{198}Au$ along the line source at the test region surface of three blankets.

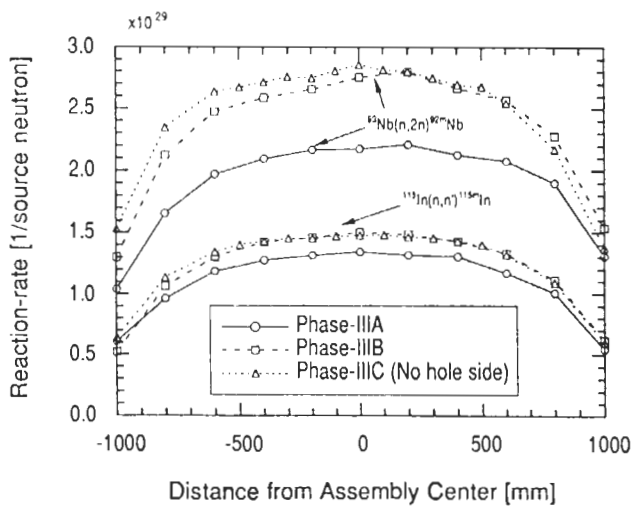

Fig. 13. Activation reaction rate distribution of $^{93}Nb(n,2n)^{92m}Nb$ and $^{115}In(n,n')^{115m}In$ along the line source at the test region surface of three blankets.

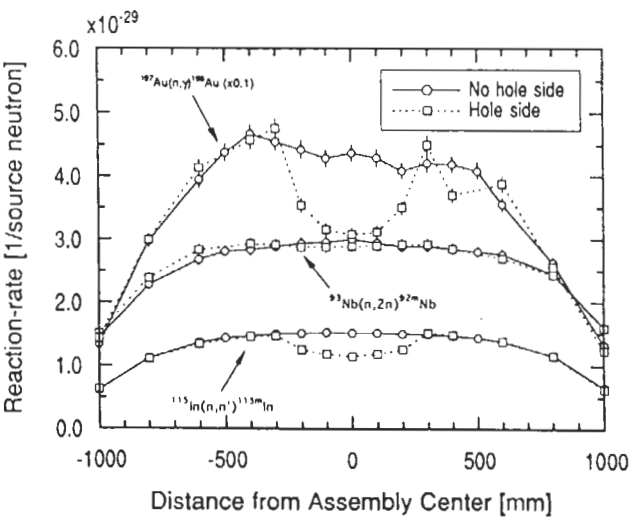

Fig. 15. Distributions of reaction rates of $^{93}Nb(n,2n)^{92m}Nb$, $^{115}In(n,n')^{115m}In$, and $^{197}Au(n,\gamma)^{198}Au$ on the graphite surface of both sides with and without an opening in the opening (Phase-IIIC) test blanket.

TABLE V

Reaction Rate Distribution Along Radial Direction at Central Drawer (Drawer B) for the Reference (Phase-IIIA) Test Blanket

Distance from the Central Axis (mm)	$^{27}Al(n,\alpha)^{24}Na$	$Ti(n,x)^{46}Sc$	$Ti(n,x)^{47}Sc$	$Ti(n,x)^{48}Sc$	$^{58}Ni(n,2n)^{57}Ni$	$^{58}Ni(n,p)^{58}Co$
213.0	---	---	---	---	---	---
231.0	4.497E−30 (3.5)[a]	5.866E−30 (4.4)	8.488E−31 (3.4)	2.119E−30 (3.3)	8.815E−31 (4.1)	1.986E−29 (3.0)
256.0	3.403E−30 (3.4)	---	---	---	---	---
281.7	2.574E−30 (3.5)	3.555E−30 (5.3)	4.682E−31 (3.6)	1.215E−30 (3.6)	4.002E−31 (4.1)	1.365E−29 (3.0)
332.2	1.533E−30 (3.6)	1.925E−30 (5.4)	2.684E−31 (3.6)	6.612E−31 (3.6)	1.933E−31 (4.9)	8.840E−30 (3.0)
382.8	8.844E−31 (3.8)	1.277E−30 (5.5)	1.622E−31 (3.6)	3.768E−31 (3.6)	9.750E−32 (7.1)	5.888E−30 (3.1)
433.3	5.351E−31 (4.0)	8.100E−31 (5.3)	1.011E−31 (3.3)	2.291E−31 (3.3)	5.227E−32 (4.5)	3.888E−30 (3.1)
484.0	---	---	---	---	---	---
535.0	---	---	---	---	---	---
585.5	1.150E−31 (4.2)	---	---	---	---	---
	$^{64}Zn(n,p)^{64}Cu$	$^{90}Zr(n,2n)^{89}Zr$	$^{93}Nb(n,2n)^{92m}Nb$	$^{115}In(n,n')^{115m}In$	$^{197}Au(n,\gamma)^{198}Au$	
213.0	---	---	---	---	1.541E−28 (6.0)	
231.0	8.836E−30 (3.5)	2.105E−29 (3.3)	1.701E−29 (2.9)	1.248E−29 (3.1)	1.590E−28 (6.2)	
256.0	---	---	---	1.089E−29 (3.0)	1.447E−28 (5.8)	
281.7	5.689E−30 (3.6)	9.866E−30 (3.3)	9.051E−30 (3.0)	8.995E−30 (3.2)	1.362E−28 (6.0)	
332.2	3.687E−30 (3.5)	4.733E−30 (3.3)	4.967E−30 (3.0)	6.602E−30 (3.3)	1.201E−28 (5.5)	
382.8	2.334E−30 (3.4)	2.465E−30 (3.3)	2.871E−30 (3.1)	4.571E−30 (3.2)	1.045E−28 (7.5)	
433.3	1.559E−30 (3.8)	1.323E−30 (3.2)	1.722E−30 (3.1)	3.277E−30 (3.3)	1.313E−28 (3.8)	
484.0	---	---	---	2.164E−30 (3.4)	1.457E−28 (5.2)	
535.0	---	---	---	1.458E−30 (3.5)	1.287E−28 (6.7)	
585.5	---	---	---	9.137E−31 (3.6)	1.310E−28 (6.4)	

[a]Read as 4.497×10^{-30} (reaction/total source neutron) with 3.5% relative error.

TABLE VI

Reaction Rate Distribution Along Radial Direction at Central Drawer (Drawer B) for the Armor (Phase-IIIB) Test Blanket

Distance from the Central Axis (mm)	$^{27}Al(n,\alpha)^{24}Na$	$Ti(n,x)^{46}Sc$	$Ti(n,x)^{47}Sc$	$Ti(n,x)^{48}Sc$	$^{58}Ni(n,2n)^{57}Ni$	$^{58}Ni(n,p)^{58}Co$
187.0	7.697E−30 (3.0)[a]	---	---	---	1.459E−30 (4.1)	3.125E−29 (3.0)
231.0	3.902E−30 (3.0)	5.409E−30 (4.3)	6.736E−31 (4.4)	1.634E−30 (3.9)	6.423E−31 (4.0)	1.932E−29 (3.0)
253.5	---	---	---	---	---	---
281.0	2.247E−30 (3.1)	3.191E−30 (4.8)	3.769E−31 (4.6)	8.700E−31 (4.1)	2.796E−31 (4.2)	1.266E−29 (3.0)
332.2	1.299E−30 (3.1)	1.876E−30 (5.2)	2.212E−31 (4.6)	4.997E−31 (4.2)	1.367E−31 (4.5)	8.260E−30 (3.0)
383.0	7.671E−31 (3.1)	1.146E−30 (6.2)	1.317E−31 (4.8)	2.876E−31 (4.4)	6.997E−32 (4.1)	5.333E−30 (3.0)
429.1	4.623E−31 (3.3)	7.343E−31 (6.6)	8.417E−32 (5.2)	1.742E−31 (4.9)	3.721E−32 (4.3)	3.525E−30 (3.0)
480.6	---	---	---	---	---	---
530.7	---	---	---	---	---	---
580.6	---	---	---	---	---	---
	$^{64}Zn(n,p)^{64}Cu$	$^{90}Zr(n,2n)^{89}Zr$	$^{93}Nb(n,2n)^{92m}Nb$	$^{115}In(n,n')^{115m}In$	$^{197}Au(n,\gamma)^{198}Au$	
187.0	---	---	2.758E−29 (3.1)	1.505E−29 (3.0)	6.630E−28 (3.2)	
231.0	7.719E−30 (3.3)	1.544E−29 (3.1)	1.340E−29 (3.1)	1.221E−29 (3.0)	3.309E−28 (3.4)	
253.5	---	---	---	1.159E−29 (3.0)	2.027E−28 (3.5)	
281.0	4.914E−30 (3.5)	7.466E−30 (3.1)	7.242E−30 (3.1)	8.707E−30 (3.1)	1.661E−28 (3.9)	
332.2	3.113E−30 (3.5)	3.672E−30 (3.2)	3.998E−30 (3.1)	6.094E−30 (3.1)	1.296E−28 (4.5)	
383.0	2.000E−30 (3.7)	1.867E−30 (3.4)	2.296E−30 (3.1)	4.181E−30 (3.0)	1.125E−28 (3.2)	
429.1	1.334E−30 (3.2)	1.045E−30 (3.6)	1.424E−30 (3.0)	2.936E−30 (3.1)	1.185E−28 (4.7)	
480.6	---	---	---	2.028E−30 (3.2)	1.365E−28 (4.3)	
530.7	---	---	---	1.303E−30 (3.2)	1.148E−28 (4.3)	
580.6	---	---	---	8.423E−31 (3.4)	1.144E−28 (4.2)	

[a]Read as 7.697×10^{-30} (reaction/total source neutron) with 3.0% relative error.

TABLE VII

Reaction Rate Distribution Along Radial Direction at Central Drawer (Drawer B) for the Opening (Phase-IIIC) Test Blanket

Distance from the Central Axis (mm)	$^{27}Al(n,\alpha)^{24}Na$	$Ti(n,x)^{46}Sc$	$Ti(n,x)^{47}Sc$	$Ti(n,x)^{48}Sc$	$^{55}Mn(n,\gamma)^{56}Mn$
187.0	---	---	---	---	---
230.0	4.185E−30 (3.4)[a]	5.125E−30 (5.1)	6.837E−31 (4.1)	1.790E−30 (4.0)	---
280.5	2.384E−30 (3.5)	2.905E−30 (5.8)	3.875E−31 (4.2)	1.015E−30 (4.2)	---
331.2	1.391E−30 (3.7)	1.833E−30 (5.5)	2.251E−31 (4.2)	5.639E−31 (4.1)	1.144E−29 (3.3)
382.0	7.843E−31 (3.8)	1.156E−30 (5.6)	1.321E−31 (4.3)	3.385E−31 (4.4)	---
428.5	4.992E−31 (3.8)	6.897E−31 (6.7)	8.597E−32 (4.1)	2.775E−31 (3.7)	---
	$Fe(n,x)^{56}Mn$	$^{59}Co(n,\alpha)^{56}Mn$	$^{58}Ni(n,2n)^{57}Ni$	$^{58}Ni(n,p)^{58}Co$	$^{64}Zn(n,p)^{64}Cu$
187.0	---	---	---	---	---
230.0	3.519E−30 (3.0)	9.564E−31 (3.2)	6.742E−31 (3.7)	1.819E−29 (2.9)	8.061E−30 (3.3)
280.5	---	---	3.164E−31 (3.8)	1.232E−29 (3.0)	5.396E−30 (3.3)
331.2	1.204E−30 (3.7)	3.070E−31 (4.1)	1.564E−31 (4.0)	8.084E−30 (3.0)	3.313E−30 (3.4)
382.0	---	---	7.415E−32 (3.6)	5.242E−30 (2.9)	2.152E−30 (3.4)
428.5	---	---	4.062E−32 (4.2)	3.475E−30 (3.0)	1.464E−30 (3.5)
	$^{90}Zr(n,2n)^{89}Zr$	$^{93}Nb(n,2n)^{92m}Nb$	$^{115}In(n,n')^{115m}In$	$^{197}Au(n,\gamma)^{198}Au$	
187.0	---	2.994E−29 (3.1)	1.514E−29 (3.1)	4.373E−28 (3.1)	
230.0	1.683E−29 (3.1)	1.547E−29 (3.1)	1.247E−29 (3.1)	2.501E−28 (3.1)	
255.0	---	---	1.028E−29 (3.1)	1.661E−28 (3.2)	
280.5	8.165E−30 (3.2)	8.451E−30 (3.1)	8.620E−30 (3.1)	1.383E−28 (3.5)	
331.2	4.100E−30 (3.2)	4.679E−30 (3.1)	5.963E−30 (3.3)	1.139E−28 (3.0)	
382.0	2.141E−30 (3.2)	2.708E−30 (3.2)	4.060E−30 (3.3)	1.066E−28 (3.1)	
428.5	1.160E−30 (3.2)	1.651E−30 (3.2)	2.874E−30 (3.4)	1.183E−28 (3.2)	
479.2	---	---	2.035E−30 (3.3)	1.298E−28 (3.2)	
530.0	---	---	1.332E−30 (3.5)	1.184E−28 (3.4)	
579.0	---	---	8.631E−31 (3.8)	1.178E−28 (3.0)	

[a]Read as 4.185×10^{-30} (reaction/total source neutron) with 3.4% relative error.

and $^{197}Au(n,\gamma)^{198}Au$ are plotted in Fig. 16 as the typical reaction rates. The reaction rates for $^{93}Nb(n,2n)^{92m}Nb$ and $^{115}In(n,n')^{115m}In$ decreased monotonously with the depth. In contrast, the gold capture reaction distributed almost in flat. The reaction rates in the armor test blanket (Phase-IIIB) decreased by 10 to 30% for threshold reactions compared with those in the reference blanket (Phase-IIIA) while the gold capture reaction rate increased by a factor of 2 at the front region, but the effect disappeared in the deeper positions. In the opening test blanket (Phase-IIIC), there is no difference from the armor test blanket (Phase-IIIB) for the threshold reactions. The gold reaction rate in Phase-IIIC is lower than that in Phase-IIIB at the front region of 200-mm depth because of a decrease of the reflected component (lower energy neutron) from the opening side.

IV.B. Comparison with Calculation

The GMVP Monte Carlo code[18] was adopted for the experimental analysis because the shapes of the Phase-III experimental assemblies were three-dimensional. This code is a vectorized version of the MORSE-DD Monte Carlo code[28] that uses a multigroup double-differential cross-section library. Because the computation speed of this vectorized version on a FACOM VP-2600 mainframe computer is 20 times faster than that of the scalar version, one can obtain reliable calculation results with large experimental assemblies such as the Phase-III experiments. The DDXLIB-J3 nuclear data library[29] of 125 groups was processed from JENDL-3 (Ref. 30). The comprehensive calculation benchmarks from these experiments are described separately for various codes and nuclear data files.[31] The line source was generated by random sampling of a point source with a uniform probability over the source length. The neutron angular emission yield and energy spectrum for the point source were taken from the results of the previous Monte Carlo calculation described in Ref. 15. The track length estimators were placed at the measurement positions. The typical neutron history was 13 000 000, and the computing time was ~1.5 h.

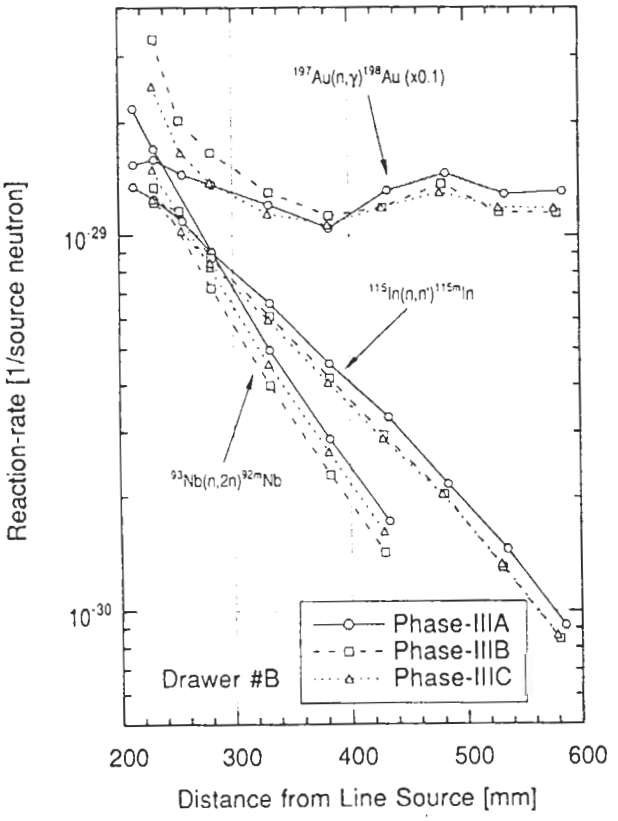

Fig. 16. Radial distributions of activation reaction rates of ^{93}Nb$(n,2n)^{92m}$Nb, ^{115}In$(n,n')^{115m}$In, and ^{197}Au$(n,\gamma)^{198}$Au in drawer B for three blankets.

The TPRs measured by the on-line methods (Li-glass and NE-213) in experimental drawer B (mid position) are compared with the calculated ones in Fig. 17 for all the test blankets. The T_7 distributions were underestimated by the calculations for all the test blankets by <10%. The calculation overestimates T_6 for the reference blanket by 5% and underestimates it for the blanket with the armor graphite by 5%. This indicates that the graphite armor provides more neutrons below the threshold energy of the ^{7}Li$(n,n'\alpha)$ reaction in the experiment than in the calculations. This is probably due to the uncertainty in the estimation of the reflected neutrons.

The calculated neutron spectra in the reference blanket (Phase-IIIA) were shown with the measured spectra in Fig. 10. In Fig. 10, an agreement is fairly good between the measurement and the calculation within 10 to 20%, although the peaks and dips by the resonances of iron and lithium in the calculated spectra are larger than those in the measured ones.

Figure 18 shows a comparison of the measured and calculated reaction rates of ^{93}Nb$(n,2n)^{92m}$Nb, ^{115}In$(n,n')^{115m}$In, and ^{197}Au$(n,\gamma)^{198}$Au along the line source on the surface of the reference test blanket (Phase-IIIA). The calculation agrees with the measured reaction rates of ^{93}Nb$(n,2n)^{92m}$Nb and ^{115}In$(n,n')^{115m}$In within 10% but underestimates the reaction rate of ^{197}Au$(n,\gamma)^{198}$Au by 30 to 40%. One possible reason for this disagreement could be the room-returned neutrons flowing in from both open

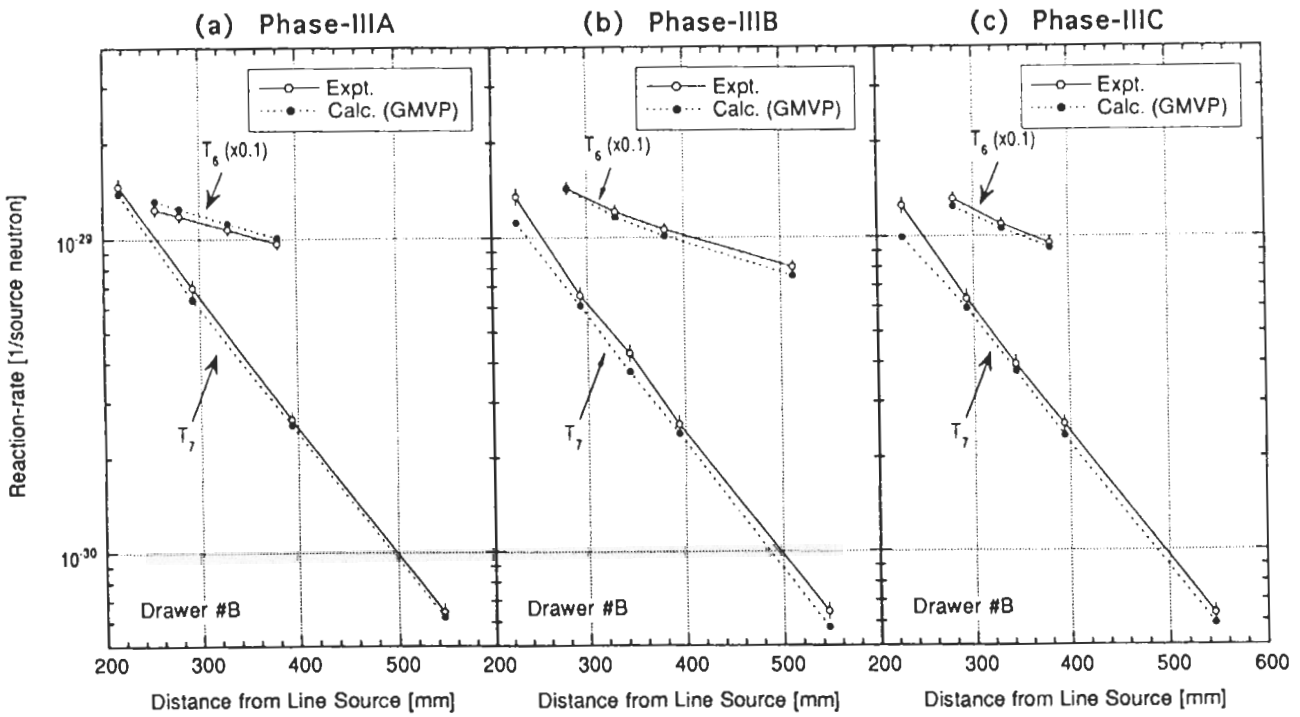

Fig. 17. Comparison between the measured and the calculated TPRs of ^{7}Li and ^{6}Li (T_7 and T_6) in drawer B for the three blankets.

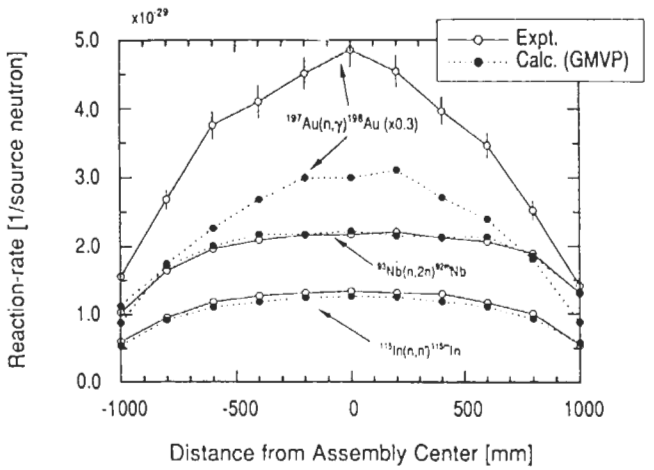

Fig. 18. Comparison between the measured and calculated activation reaction rates of $^{93}Nb(n,2n)^{92m}Nb$, $^{115}In(n,n')^{115m}In$, and $^{197}Au(n,\gamma)^{198}Au$ along the line source at the test region surface for the reference blanket (Phase-IIIA).

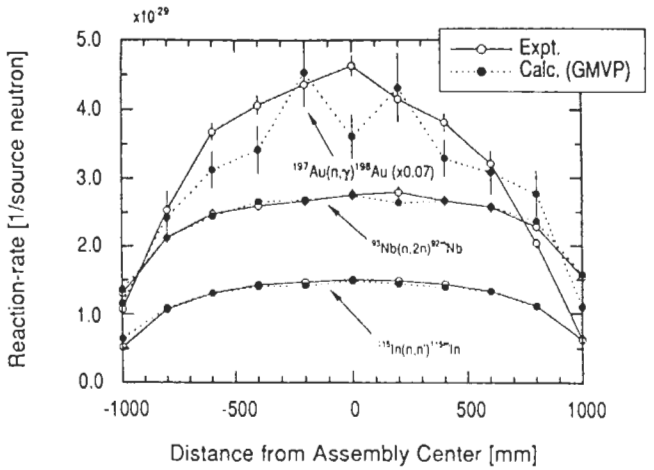

Fig. 19. Comparison between the measured and calculated activation reaction rates of $^{93}Nb(n,2n)^{92m}Nb$, $^{115}In(n,n')^{115m}In$, and $^{197}Au(n,\gamma)^{198}Au$ along the line source at the test region surface for the armor blanket (Phase-IIIB).

ends of the cavity. This discrepancy decreases in the Phase-IIIB assembly, as shown in Fig. 19, because lower energy neutrons increased at the graphite armor and the influence of the background neutrons decreased relatively.

The calculation also showed good agreement with the measured threshold reaction rates along the radial direction within 10%, as shown in Fig. 20, while the discrepancy was >20% for the reaction rate of $^{197}Au(n,\gamma)^{198}Au$. The tendency between the measured

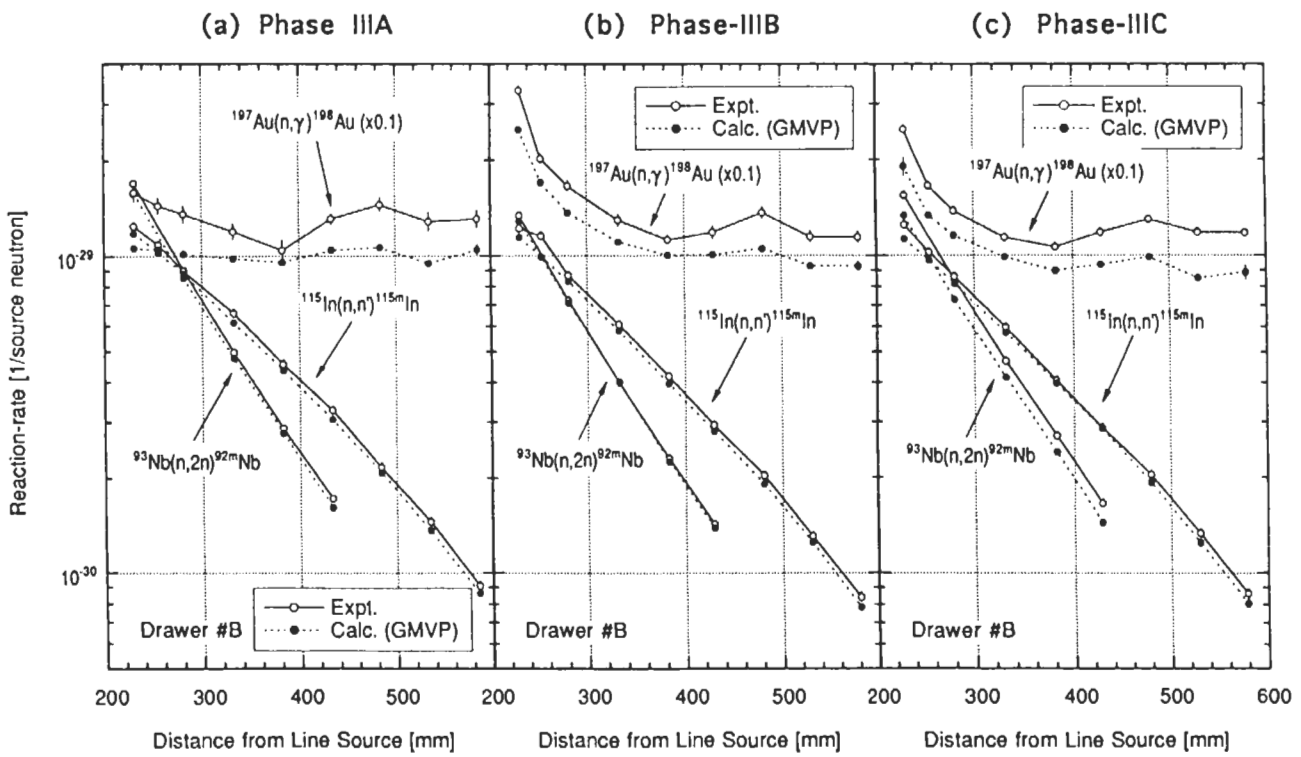

Fig. 20. Comparison between the measured and calculated activation reaction rates of $^{93}Nb(n,2n)^{92m}Nb$, $^{115}In(n,n')^{115m}In$, and $^{197}Au(n,\gamma)^{198}Au$ in drawer B for the three blankets.

and the calculated reaction rates for the high-threshold reactions was very similar to that for T_7.

Overall, the GMVP Monte Carlo code calculation with JENDL-3 agreed with the measured reaction rates and TPRs within 10% and with the measured neutron spectrum within 20% for all the blankets in spite of very complicated blanket configurations.

V. CONCLUSION

Neutron spectra, TPRs, and activation reaction rates were measured in annular blanket systems with a pseudoline D-T neutron source. The systems were performed for the reference (first wall/Li_2O/Li_2CO_3/polyethylene), the armor (carbon/first wall/Li_2O/Li_2CO_3/polyethylene), and the large opening (the armor configuration with an opening at the center) configurations of the test blankets.

In the current geometry, the D-T neutron source spectrum incident to the blanket was broader for the line source than the point D-T neutron source spectrum and gave better simulation for the neutron spectrum from a D-T plasma. The graphite armor increased significantly low-energy neutrons inside the inner cavity and increased TPR from ^{6}Li in the front region of the blanket. The opening decreased low-energy neutrons contained in the cavity and especially decreased TPR from ^{6}Li in the blanket at the opposite side. The GMVP Monte Carlo code that uses the JENDL-3 nuclear data library can predict the measured nuclear parameters such as TPR in the test blankets within an accuracy of 10%.

The neutronic environments examined in this work would frequently appear in the environment of a fusion reactor, and the current results suggest that the nuclear parameters of the components around the plasma are very sensitive to the configuration. Hence, the current data can play a role as basic data for a higher step of a benchmark study, i.e., a prototypical reactor test to examine the overall ability of neutronics calculations for a realistic reactor.

ACKNOWLEDGMENTS

The authors would like to thank J. Kusano, C. Kutsukake, S. Tanaka, and Y. Abe for their excellent operation of the FNS accelerator system. The U.S. work was supported by the U.S. DOE Office of Fusion Energy.

REFERENCES

1. H. MAEKAWA et al., "Fusion Blanket Benchmark Experiments on a 60 cm-Thick Lithium Oxide Cylindrical Assembly," JAERI-M 86-182, Japan Atomic Energy Research Institute (1986).

2. Y. OYAMA and H. MAEKAWA, "Measurement and Analysis of an Angular Neutron Flux on a Beryllium Slab Irradiated with Deuterium-Tritium Neutrons," *Nucl. Sci. Eng.*, **97**, 220 (1987).

3. A. TAKAHASHI, M. KAWATA, and A. MASAGO, "Tritium Breeding Experiment for a Thermal Blanket Model of Pb-Li-C," *Fusion Eng. Des.*, **9**, 333 (1989).

4. T. NAKAMURA and M. A. ABDOU, "Summary of Recent Results from the JAERI/U.S. Fusion Neutronics Phase I Experiments," *Fusion Technol.*, **10**, 541 (1986).

5. M. Z. YOUSSEF, C. GUNG, M. NAKAGAWA, T. MORI, K. KOSAKO, and T. NAKAMURA, "Analyses and Intercomparison for Phase I Fusion Integral Experiments at the FNS Facility," *Fusion Technol.*, **10**, 549 (1986).

6. Y. OYAMA, Y. IKEDA, T. MORI, M. NAKAGAWA, T. NAKAMURA, and H. MAEKAWA, "Neutron Field Characteristics in a Concrete Cavity Having a DT Neutron Source," *Fusion Technol.*, **10**, 585 (1986).

7. H. MAEKAWA et al., "Measured Neutron Parameters for Phase I Experiments at the FNS Facility," *Fusion Technol.*, **10**, 564 (1986).

8. Y. OYAMA et al., *Fusion Eng. Des.*, **9**, 309 (1989); see also Y. OYAMA et al., "Phase II-B Experiment of JAERI US/DOE Collaborative Program on Fusion Blanket Neutronics," *Fusion Technol.*, **15**, 1293 (1989); see also "Phase IIA and IIB Experiments of JAERI/U.S. DOE Collaborative Program on Fusion Blanket Neutronics – Experimental Results," JAERI-M 89-215, Japan Atomic Energy Research Institute (1989).

9. M. NAKAGAWA, T. MORI, K. KOSAKO, Y. OYAMA, and T. NAKAMURA, "JAERI/U.S. DOE Collaborative Program on Fusion Blanket Neutronics – Analysis of Phase IIA and IIB Experiments," JAERI-M 89-154, Japan Atomic Energy Research Institute (1989).

10. M. Z. YOUSSEF, M. A. ABDOU, Y. WATANABE, and P. M. SONG, "U.S./JAERI Collaborative Program on Fusion Neutronics – Phase IIA and IIB Fusion Integral Experiments, The U.S. Analysis," UCLA-ENG-90-14, FNT-31, University of California, Los Angeles (1990).

11. M. NAKAGAWA et al., "Analysis of Neutronics Parameters Measured in Phase II Experiments of the JAERI/U.S. Collaborative Program on Fusion Blanket Neutronics, Part 1," *Fusion Eng. Des.*, **9**, 315 (1989).

12. M. Z. YOUSSEF et al., "Analysis of Neutronics Parameters Measured in Phase II Experiments of the JAERI/U.S. Collaborative Program on Fusion Blanket Neutronics, Part II," *Fusion Eng. Des.*, **9**, 323 (1989).

13. Y. OYAMA et al., "Measured Characteristics of Be Multi-Layered and Coolant Channel Blankets: Phase IIC Experiments of the JAERI/U.S. DOE Collaborative Program on Fusion Neutronics," *Fusion Technol.*, **19**, 1955 (1991); see also "Phase IIC Experiments of the JAERI/US

DOE Collaborative Program on Fusion Blanket Neutronics, Volume 1: Experimental Results," JAERI-M 92-182, Japan Atomic Energy Research Institute; see also UCLA-ENG-93-18, University of California, Los Angeles (1992).

14. M. Z. YOUSSEF, A. KUMAR, M. ABDOU, M. NAKAGAWA, K. KOSAKO, Y. OYAMA, and T. NAKAMURA, "Analysis for Heterogeneous Blankets and Comparison to Measurements: Phase IIC Experiments of the U.S. DOE/JAERI Collaborative Program on Fusion Neutronics," *Fusion Technol.*, **19**, 1891 (1991); see also "Phase IIC Experiments of the U.S./JAERI Collaborative Program on Fusion Blanket Neutronics, Volume 2: Analysis," UCLA-ENG-93-19, University of California, Los Angeles; see also JAERI-M 92-183, Japan Atomic Energy Research Institute (1992).

15. Y. OYAMA et al., "Concept and Characteristics of a Simulated Line Source for Annular Blanket Experiments Using an Accelerator-Based Deuterium-Tritium Neutron Source," *Fusion Technol.*, **28**, 305 (1995).

16. Y. OYAMA et al., "Annular Blanket Experiment Using a Line D-T Neutron Source: Phase IIIA of the JAERI/U.S. DOE Collaborative Program on Fusion Neutronics," *Fusion Technol.*, **19**, 1879 (1991).

17. Y. OYAMA et al., "Phase III Experimental Results of JAERI/U.S. DOE Collaborative Program on Fusion Neutronics," *Fusion Eng. Des.*, **18**, 203 (1991).

18. T. MORI et al., "Vectorization of Continuous Energy Monte Carlo Method for Neutron Transport Calculation," *J. Nucl. Sci. Technol.*, **29**, 325 (1992).

19. T. NAKAMURA, H. MAEKAWA, Y. IKEDA, and Y. OYAMA, "A D-T Neutron Source for Fusion Neutronics Experiments at the JAERI," *Proc. 7th Symp. (1983 Int.) Ion Sources and Ion-Assisted Technology (ISIAT' 83) and 4th Int. Conf. Ion and Plasma-Assisted Techniques (IPAT' 83)*, Kyoto, Japan, September 12–16, 1983, p. 567, Institute of Electrical Engineers of Japan.

20. H. MAEKAWA et al., "Neutron Yield Monitors for the Fusion Neutronics Source (FNS)," JAERI-M 84-193, Japan Atomic Energy Research Institute (1984).

21. T. KURODA et al., "ITER Plasma-Facing Components," ITER Documentation Series No. 30, International Atomic Energy Agency (1991).

22. S. YAMAGUCHI et al., "An On-Line Method for Tritium Production Measurement with a Pair of Lithium-Glass Scintillators," *Nucl. Instrum. Methods*, **A254**, 413 (1987).

23. Y. OYAMA et al., "A Small Spherical NE213 Scintillation Detector for Use in In-Assembly Fast Neutron Spectrum Measurements," *Nucl. Instrum. Methods*, **A256**, 333 (1987).

24. E. F. BENNETT and T. J. YULE, "Techniques and Analyses of Fast Reactor Neutron Spectroscopy with Proton-Recoil Proportional Counters," ANL-7763, Argonne National Laboratory (1971).

25. E. F. BENNETT, "A Continuous Mode Data Acquisition Technique for Proton Recoil Proportional Counter Neutron Spectrometers," ANL/FPP/TM-239, Argonne National Laboratory (1989).

26. Y. OYAMA, K. SEKIYAMA, and H. MAEKAWA, "Spectrum Weighting Function Method for In-Situ Fast Neutron and Gamma-Ray Response Measurements in Fusion Integral Experiments with an NE-213 Scintillation Detector," *Proc. 11th Topl. Mtg. Technology of Fusion Energy*, New Orleans, Louisiana, June 19–23, 1994, *Trans. Fusion Technol.*, **26**, 1098 (1994).

27. "FORIST Spectrum Unfolding Code," PSY-92, Radiation Shielding Information Center, Oak Ridge National Laboratory (1975).

28. M. NAKAGAWA and T. MORI, "MORSE-DD, A Monte Carlo Code Using Double Differential Form Cross Sections," JAERI-M 84-126, Japan Atomic Energy Research Institute (1984).

29. T. MORI, Japan Atomic Energy Research Institute, Private Communication (1992).

30. K. SHIBATA et al., "Japanese Evaluated Nuclear Data Library, Version-3," JAERI 1319, Japan Atomic Energy Research Institute (1990).

31. M. Z. YOUSSEF et al., "The Nuclear Analysis of an Annular Li_2O Blanket System Surrounding an Artificially Simulated 14-MeV Line Source and Comparison of Calculations to Measurements," *Fusion Technol.*, **28**, 320 (1995).

Chikara Konno (MS, physics, Kyoto University, Japan, 1985) is a research scientist in the Department of Reactor Engineering at the Japan Atomic Energy Research Institute (JAERI). He has worked in the areas of fusion neutronics experiments, cross-section measurements, and neutron spectrum measurements using a proton-recoil counter.

Yukio Oyama (BS, physics, 1975; MS, nuclear physics, 1977; and Dr. Eng., 1989, Osaka University, Japan) is a principal scientist at JAERI. He has worked in the area of fusion neutronics experiments since 1978. He is currently involved in intense and high-energy neutron source projects.

Fujio Maekawa (MS, nuclear engineering, Osaka University, Japan, 1990) is a research scientist at JAERI. He has been engaged in integral experiments for fusion neutronics and studied the behavior of neutron, photon, and electron transport in media. His current interests are in the measurements of tritium and decay heat of irradiated materials.

Yujiro Ikeda (PhD, nuclear engineering, Nagoya University, Japan, 1981) is head of the Fusion Neutronics Laboratory in the Department of Reactor Engineering at JAERI. He has worked in the areas of fusion neutronics experiments, induced radioactivity experiment and analysis, direct nuclear heating measurements, activation cross-section measurements, and fusion dosimetry.

Kazuaki Kosako (BE, atomic engineering, Tokai University, Japan, 1984) has worked at Sumitomo Atomic Energy Industries since 1994. He worked in the Department of Reactor Engineering at JAERI from 1984 to 1992 where he was involved mainly in fusion neutronics. He is currently interested in the area of radiation damage of materials.

Hiroshi Maekawa (BE, 1965; MS, 1967; and Dr. Eng., 1970, nuclear engineering, Tokyo Institute of Technology, Japan) is the deputy director of the Department of Reactor Engineering and the head of the Intense Neutron Source Laboratory at JAERI. He has worked on fusion neutronics for more than 20 years, and he planned and constructed the Fusion Neutronics Source (FNS) facility. He served as the Japanese leader of the JAERI/U.S. Department of Energy (U.S. DOE) collaboration on fusion blanket neutronics. His recent research has focused on International Fusion Materials Irradiation Facility conceptual design activities.

Mohamed A. Abdou is a professor in the Department of Mechanical, Aerospace, and Nuclear Engineering at the University of California, Los Angeles (UCLA) and also is the director of fusion technology at UCLA. His research interests include neutronics, thermomechanics, fusion technology, and reactor design and analysis. He served as the U.S. leader of the JAERI/U.S. DOE collaboration on fusion blanket neutronics.

Edgar F. Bennett (PhD, University of New Hampshire, 1957) is a physicist at Argonne National Laboratory. He has been a section head of experimental reactor physics since 1970. He is best known as the inventor of a widely used in-core proton-recoil spectrometer—a technique that he has been continually updating. He has also made contributions to the field of reactivity measurement by reactor noise techniques, in particular, by providing a common theoretical basis and introducing a new type of variance experiment.

Anil Kumar (PhD, University of Bombay, India, 1981) is senior development engineer at UCLA. His current research interests include fusion reactor nucleonics experiments and analysis, technique development for nuclear heating, decay heat measurements, biological dose, fusion diagnostics, safety factor methodology for fusion reactor design parameters, low-activation materials, inertial confinement fusion, and sequential reactions. He has conducted experiments at leading facilities such as the FNS facility in Japan, the Tokamak Fusion Test Reactor (TFTR) at Princeton University, and LOTUS in Switzerland.

Mahmoud Z. Youssef (PhD, nuclear engineering, University of Wisconsin, 1980) is a senior research engineer in the Department of Mechanical, Aerospace, and Nuclear Engineering at UCLA. He participated in several conceptual magnetic fusion energy and inertial fusion energy reactor design studies with emphasis on nuclear analysis and blanket/shield design. His research interests are in the areas of blanket/shield design optimization, nuclear data, sensitivity/uncertainty studies, neutronics methods and code development, tritium fuel cycle, radioactivity and safety aspects of fusion, integral experiments, neutronics testing, and research and development for fusion reactors, particularly the International Thermonuclear Experimental Reactor (ITER).